FAR FIELD BOUNDARY CONDITIONS FOR INCOMPRESSIBLE FLOWS COMPUTATION

Charles-Henri Bruneau[1,†] and Sandra Tancogne[2]

Abstract Many far field boundary conditions are proposed in the literature to solve Navier-Stokes equations. It is necessary to distinguish the streamwise or outlet boundary conditions and the spanwise boundary conditions. In the first case the flow crosses the artificial frontier and it is required to avoid reflections that can change significantly the flow. In the second case the Navier-slip boundary condition is often used but if the frontier is not far enough the boundary is both inlet and outlet. Thus the Navier-slip boundary condition is not well suited as it imposes no flux through the frontier. The aim of this work is to compare some well-known boundary conditions, to quantify to which extend the artificial frontier can be close to the bodies in two- and three-dimensions and to take into account the flow rate through the spanwise directions.

Keywords Navier-Stokes equations, far field boundary conditions, flow rate conservation.

MSC(2010) 65M55, 76D05.

1. Introduction

In many incompressible flow problems, in particular when the flow around obstacles is concerned, we have to specify boundary conditions on artificial frontiers to solve the Navier-Stokes equations. But there is two kind of artificial frontiers: the streamwise or outlet boundaries and the spanwise boundaries. In the first case the flow crosses the artificial frontier and it is required to avoid reflections that can change significantly the flow even if the frontier is far away. In the second case if the frontier is far enough it is often considered that the flow is tangent to the boundary and thus the Navier-slip boundary condition is used. However if the frontier is not far enough the boundary is both inlet and outlet. Thus the Navier-slip boundary condition is not well suited any more as it imposes no flux through the frontier. Indeed, the flow rate at the outlet boundary is equal to the flow rate at the entrance section, which is not the case.

In the literature there are many authors who propose efficient boundary conditions, specially in the first case that includes channel flows. Dirichlet and Neumann boundary conditions are not concerned as they induce strong reflections from the

---

†the corresponding author.

  Email address:bruneau@math.u-bordeaux.fr (C.-H. Bruneau)

[1]Univ. Bordeaux IMB, INRIA Bordeaux Sud-Ouest MEMPHIS, CNRS UMR5251, F-33405 Talence, France

[2]Univ. de Reims Champagne-Ardenne, Laboratoire de Mathématiques B.P. 1039, F-51687 Reims, France

frontier unless the frontier is very far away or they are coupled to a sponge proce-
dure [12] which is not investigated in this work. Following some pioneering works
(see for instance [14] and [7]) many researchers have proposed outlet boundary con-
ditions that can be classified into four types: the convective boundary conditions
(see [10, 15] and references therein), the Navier-slip boundary conditions [11, 16],
the traction or directional do-nothing boundary conditions [2, 3, 8, 18] and the open
boundary conditions involving transformed, parabolized or reduced Navier-Stokes
equations [6, 9, 13, 17]. In most cases these boundary conditions are used to derive
the velocity or the pressure or both in ghost cells outside the domain to be able to
compute the flow in the last cells of the domain. In some cases the divergence-free
condition is coupled to the boundary conditions and sometimes the flow rate is
taken into account to avoid mass loss.

On spanwise far field frontiers the researchers use either one of the boundary
conditions above or Dirichlet, Neumann or extrapolated boundary conditions. In
most cases the frontier is quite far away and even Dirichlet boundary condition with
the flow at infinity is relevant as well as the Navier-slip boundary condition. But
in both cases the boundary condition implies there is no flux through the frontier.
Which is not correct if the frontier is closer to the obstacle. Indeed, in such case,
the spanwise frontier is partly outlet in front of the body and partly inlet behind.
So it is crucial to let the flow free to leave or to enter the domain. Thus most of the
boundary conditions are not useful. The goal of this work is to find out the best
boundary condition on spanwise frontiers that allows to restrict the computational
domain as close as possible to the obstacle and to quantify the error with respect
to the distance of the frontier to the obstacle for various Reynolds numbers. The
computations are performed around an horizontal bar set down on a solid wall in
two- and three-dimensions. The results show that the error is linked to the blockage
ratio of the bar section to the domain section.

This paper is organised in four sections in addition to this introduction. The
first one is devoted to the Modelling and numerical simulations. The second one
describes the various boundary conditions. In the third section the numerical results
in two-dimensions are presented. The fourth section is devoted to the results in
three-dimensions. At the end some conclusions are provided.

2. Modelling and numerical simulations

In this section, the method used to simulate the flow past full scale Ahmed bodies
on top of a road using Cartesian grids is presented. To compute the flow around
solid bodies an immersed boundary model is used, namely the penalized Navier-
Stokes equations for the velocity and pressure (U, p) as unknowns [1] ($U = (u, w)$ in
two-dimensions and $U = (u, v, w)$ in three-dimensions). The non dimensional form
is based on the far field velocity of the flow U_∞ and the height H of Ahmed body,
these equations read:

$$\partial_t U + (U \cdot \nabla)U - \frac{1}{Re}\Delta U + \frac{U}{K} + \nabla p = 0 \ \text{ in } \Omega_T = \Omega \times (0, T), \qquad (2.1)$$

$$\nabla \cdot U = 0 \ \text{ in } \Omega_T, \qquad (2.2)$$

where $Re = \frac{|U_\infty|H}{\nu}$ is the non dimensional Reynolds number associated to the kine-
matic viscosity of the fluid ν, $K = \frac{k|U_\infty|}{\nu \Phi H} = \frac{kRe}{\Phi H^2}$ is the non dimensional coefficient

of permeability of the medium representing the bodies with k the intrinsic permeability and Φ the porosity of the medium, Ω is the full domain including the solid bodies and T is the simulation time. In the fluid domain the permeability coefficient goes to infinity, the penalization term vanishes and we solve the genuine non dimensional Navier-Stokes equations. In the solid body the permeability coefficient goes to zero, so U/K is large and dominate other velocity terms that become negligible. It has been shown in [1] that solving these equations corresponds to solve Darcy's law in the solid parts and that the velocity is proportional to K. For numerical simulations we set $K = 10^{16}$ in the fluid and $K = 10^{-8}$ in the solid bodies. In the non dimensional form of the equations the time is $t = t_r \mid U_\infty \mid /H$ and the pressure is $p = p_r/(\rho_r \mid U_\infty \mid^2)$ where the subscript r stands for the real values. The
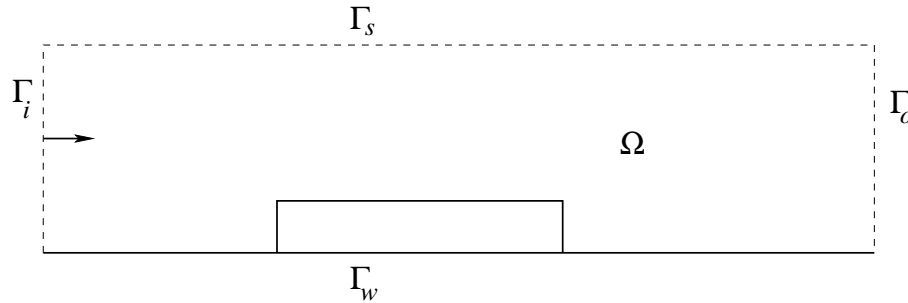

Figure 1. Computational domain in two-dimensions.

equations (2.1), (2.2) above are solved in a computational domain (Figure 1) and are associated to an initial datum ($X = (x, z)$ in two-dimensions and $X = (x, y, z)$ in three-dimensions):

• $U(X, 0) = U_0(X)$ in Ω

and to the following boundary conditions:

• $U = U_\infty = (1, 0)$ or $(1, 0, 0)$ at the entrance section Γ_i;

• $U = 0$ on the wall Γ_w;

• a boundary condition to be precised on the longitudinal far field boundary Γ_s;

• $\sigma(U, p)n + \frac{1}{2}(U \cdot n)^-(U - U_{ref}) = \sigma(U_{ref}, p_{ref})n$ on the exit downstream boundary Γ_o where $\sigma(U, p) = 1/Re(\nabla U + \nabla U^t) - pI = 2\nu D(U) - pI$ is the stress tensor, n is the unit normal pointing outside of the domain and the notation $a = a^+ - a^-$ is used. This boundary condition conveys properly the vortices downstream as shown in [3] and in the Figure 2 for two different length of the domain in two-dimensions. After $10,000$ time iterations some discrepancies begin to appear but this is also the case when computing on different number of cores or when the real numbers are stored on a different way on the computers. The result shows both that there is no reflections and that it is possible to cut the domain close to the obstacle downstream. Of course, even if the instantaneous flow becomes different, the mean flow is the same.

Then a simulation is performed using a second-order Gear scheme in time with explicit treatment of the convection term. All the linear terms are treated implicitly and discretized via a second-order centred finite differences scheme. The Courant-Friedrichs-Lewy condition related to the convection term requires a time step of the order of magnitude of the space step as U is of order one. A third-order finite
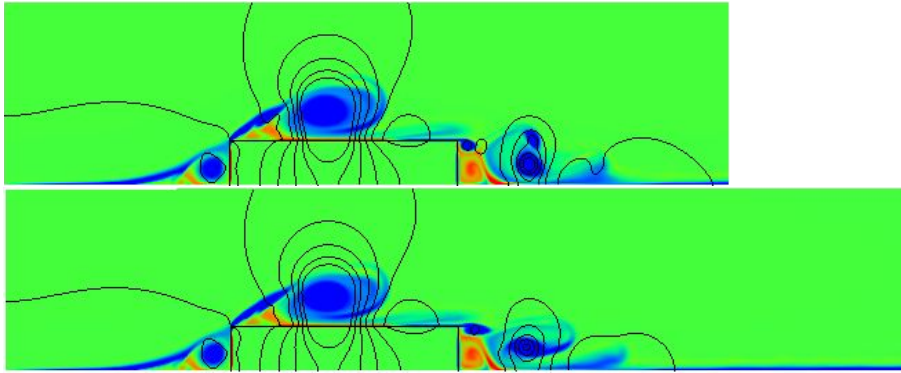
Figure 2. Vorticity field in colours and pressure contours in black lines of the instantaneous flow by a long bar at $Re = 10,000$ after $10,000$ time iterations in two domains of different length.

differences upwind scheme is used for the space discretization of the convection terms [5]. The efficiency of the resolution is obtained by a multigrid procedure using a cell-by-cell Gauss-Seidel smoother. For each cell in 3D, it consists in reversing the 7×7 matrix:

$$
\begin{pmatrix}
a_{11} & 0 & 0 & 0 & 0 & 0 & \frac{1}{\delta x} \\
0 & a_{22} & 0 & 0 & 0 & 0 & -\frac{1}{\delta x} \\
0 & 0 & a_{33} & 0 & 0 & 0 & \frac{1}{\delta y} \\
0 & 0 & 0 & a_{44} & 0 & 0 & -\frac{1}{\delta y} \\
0 & 0 & 0 & 0 & a_{55} & 0 & \frac{1}{\delta z} \\
0 & 0 & 0 & 0 & 0 & a_{66} & -\frac{1}{\delta z} \\
-\frac{1}{\delta x} & \frac{1}{\delta x} & -\frac{1}{\delta y} & \frac{1}{\delta y} & -\frac{1}{\delta z} & \frac{1}{\delta z} & 0
\end{pmatrix}
\begin{pmatrix}
u_{i-\frac{1}{2},j,k} \\
u_{i+\frac{1}{2},j,k} \\
v_{i,j-\frac{1}{2},k} \\
v_{i,j+\frac{1}{2},k} \\
w_{i,j,k-\frac{1}{2}} \\
w_{i,j,k+\frac{1}{2}} \\
p_{i,j,k}
\end{pmatrix}
=
\begin{pmatrix}
b_1 \\
b_2 \\
b_3 \\
b_4 \\
b_5 \\
b_6 \\
b_7
\end{pmatrix}
\tag{2.3}
$$

with $(a_{ii})_{1 \leq i \leq 6}$ the diagonal composed of the time term, the diagonal of the linear diffusion terms and the penalization term, and $(b_i)_{1 \leq i \leq 7}$ the second member made of all the remaining terms including the non-linear convection terms and the second member of the equation if any.

The computational domain is $\Omega = (0\,,16) \times (0\,,h)$ in two-dimensions and $\Omega = (0\,,16) \times (0\,,h) \times (0\,,h)$ in three-dimensions where the height of the computational domain take the values $4, 8, 16, 32, 64, 128$ in two-dimensions and $4, 8, 16$ in three-dimensions. the horizontal bar is of length 5 from 5 to 10 in the x-direction and of height and width 1.

The computational time is reduced using an efficient MPI parallelism [4]. The main difficulties are linked to the multigrid solver, on the one hand because of the cell-by-cell Gauss-Seidel smoother and not Jacobi smoother and, on the other hand due to the multigrid itself that uses very coarse grids that can not be computed in parallel. Nevertheless the computational code can run on 384 cores in 3D with a strong scalability close to one [4].

The results are presented at $Re = 100$, $Re = 1,000$ and $Re = 10,000$ based on the bar height H for all the numerical simulations to achieve several flow regimes.

To insure the reliability of the results, the simulations are performed on six uniform grids starting from a coarse $16 \times h$ or $16 \times h^2$ cells mesh to a fine $512 \times 32h$ or $512 \times 1024h^2$ cells mesh on which grid convergence is reached. The numerical simulations use a time step $\delta t = 2.10^{-3}$ that corresponds to the Courant-Friedrichs-Lewy condition on the finest grid. In addition the simulation time is large enough for the flow crosses the domain several times in order to get realistic mean flows. The physical quantities are computed using either a direct computation or the penalization term. Indeed the drag and lift forces are given by:

$$F_D = - \int_{body} \partial_x p \, dX \; + \int_{body} \tfrac{1}{Re} \Delta u \, dX \approx \int_{body} \frac{u}{K} \, dX,$$

$$F_L = - \int_{body} \partial_z p \, dX \; + \int_{body} \tfrac{1}{Re} \Delta w \, dX \approx \int_{body} \frac{w}{K} \, dX.$$

Then the drag coefficient C_D and the lift coefficient C_L are computed as usual:

$$C_D = 2F_D/S \;\; , \;\; C_L = 2F_L/S,$$

where S is the cross section of the body. In two-dimensions $S = H$ and in three-dimensions $S = H^2$. The flow rate across a vertical section of the computational domain, the profile of the velocity and the drag coefficient are presented throughout the paper.

3.   Boundary conditions

In this section the boundary conditions used to solve Navier-Stokes or Stokes equations in domains with artificial frontiers are sometimes formulated in two-dimensions for the sake of simplicity. As stated in the introduction there are four types of boundary conditions in addition to Dirichlet and Neumann boundary conditions. They are mainly used to determine the flow in ghost cells outside the computational domain.

- The convective boundary conditions are often written [10, 15]:

$$\partial_t u + (\overline{U} \cdot \nabla)u = 0 \;\; \text{on } \Gamma_s,$$
$$w = 0 \;\; \text{on } \Gamma_s,$$

$$(3.1)$$

where $\overline{U}$ is chosen by the user according to the local flow. These conditions are not well suited on Γ_s when the frontier is close to the body as the second condition on w prevent the flow to leave or enter the domain as it is required.

- The Navier-slip or Navier-friction boundary conditions are written [11]:

$$\nu \, \tau \cdot D(U)n + \gamma u = \nu \, \partial_z u + \gamma u = 0 \;\; \text{on } \Gamma_s,$$
$$w = 0 \;\; \text{on } \Gamma_s,$$

$$(3.2)$$

where $\nu = 1/Re$, τ is the unit tangent vector and γ is a positive friction coefficient. Once again the slip condition is not convenient.

- The traction boundary condition is written in its simplest form [18]:

$$\sigma(U, p)n = \sigma(U_{ref}, p_{ref})n \;\; \text{on } \Gamma_s,$$

$$(3.3)$$

where the reference flow (U_{ref}, p_{ref}) is often taken in such a way that the second member is equal to zero. This condition or the complete form used above on Γ_o can be used on the spanwise boundaries. Let us point out that when the reference flow is updated along time it can be necessary to control the flow rate.

• The open boundary conditions can take various forms including Neumann boundary conditions, second derivative set to zero or a parabolized form that couples velocity and pressure as:

$$-1/Re\partial_n^2 u + \partial_\tau p = -1/Re\partial_z^2 u + \partial_x p = 0 \ \ \text{on } \Gamma_s,$$
$$-1/Re\partial_\tau^2 w + \partial_n p = -1/Re\partial_x^2 w + \partial_z p = 0 \ \ \text{on } \Gamma_s. \tag{3.4}$$

These equations as well as the traction one can be coupled to the divergence-free condition to get the three unknowns (in two-dimensions) in ghost cells.

As it is required that the flow can leave or enter the domain through the spanwise frontiers, only the two last sets of equations are considered in the following. To precise how the boundary conditions are really computed in a ghost cell a staggered cell and its ghost neighbour are represented in Figure (3). Moreover, as there are Cartesian uniform grids $\delta x = \delta y = \delta z = \delta$ and thus some formula are simplified, the value of u_1 is always determined the same way than u_0.
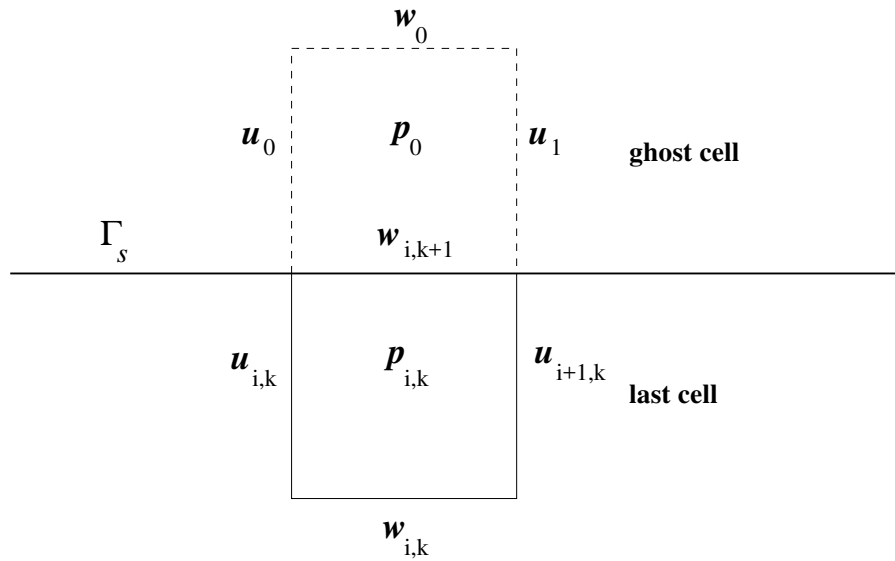

Figure 3. Values u_0, u_1, w_0 and p_0 in a ghost cell in two-dimensions.

The boundary conditions used for comparison are the following:
• The Neumann boundary condition

$$u_0 = u_{i,k}, \ w_0 = w_{i,k+1}, \ p_0 = p_{i,k}. \tag{3.5}$$

Eventually w_0 can be derived using the divergence free condition as:

$$w_0 = w_{i,k+1} - (u_1 - u_0). \tag{3.6}$$

This is permissible as the continuity equation is valid everywhere.

- The linear extrapolation

$$u_0 = 2u_{i,k} - u_{i,k-1}, \ w_0 = 2w_{i,k+1} - w_{i,k}, \ p_0 = 2p_{i,k} - p_{i,k-1}. \tag{3.7}$$

- The traction and divergence-free conditions with the reference flow (U_{ref}, p_{ref}) taken equal to the flow on the previous cell $(U_{i,k-1}, p_{i,k-1})$ just computed by the cell-by-cell smoother.

$$\begin{aligned}
u_0 =& u_{i,k} - (w_{i,k+1} - w_{i-1,k+1}) + (u_{i,k} - u_{i,k-1}) + (w_{i,k} - w_{i-1,k}) \\
& - \delta/4 \ Re \ \mathrm{Min}(w^{m-1}_{i-1,k+1} + w^{m-1}_{i,k+1}, 0)(u^{m-1}_{i,k} - u_{i,k-1}), \\
w_0 =& w_{i,k+1} - (u_1 - u_0), \\
p_0 =& p_{i,k} + 2(u_1 - u_0)/(Re\delta) - 2(u_{i+1,k} - u_{i,k})/(Re\delta) \\
& - 1/4 \ \mathrm{Min}(w^{m-1}_{i,k+1} + w^{m-1}_0, 0)((w^{m-1}_{i,k+1} + w^{m-1}_0) - (w_{i,k} + w_{i,k+1})),
\end{aligned} \tag{3.8}$$

where the exponent $m-1$ stands for the previous iterate in time as the convection term is treated explicitly.

- The parabolized Stokes equations and divergence-free condition

$$\begin{aligned}
u_0 &= u_{i,k} + (u_{i,k} - u_{i,k-1}) + (Re\delta)(p_{i,k} - p_{i-1,k}), \\
w_0 &= w_{i,k+1} - (u_1 - u_0), \\
p_0 &= p_{i,k} + (w_{i+1,k+1} - 2w_{i,k+1} + w_{i-1,k+1})/(Re\delta).
\end{aligned} \tag{3.9}$$

In some sense the equations (3.7), (3.8) and (3.9) can be seen as variations of the Neumann boundary conditions (3.5).

4. Numerical results in two-dimensions

The two-dimensional flow around a long bar $(5, 10) \times (0, 1)$ of height $H = 1$ is simulated in the computational domain $\Omega = (0, 16) \times (0, h)$ where h takes the values $h = 4$, $h = 8$, $h = 16$, $h = 32$, $h = 64$ and $h = 128$. These values correspond to a blockage of the computational domain by the bar $b = 1/h$ and the case $h = 128$ is referred as the reference flow. The study concerns three different Reynolds numbers $Re = 100$, $Re = 1,000$ and $Re = 10,000$ corresponding to three different regimes as shown in Figure 4. There is a steady solution at $Re = 100$ and two solutions in transitions to turbulence at $Re = 1,000$ and $Re = 10,000$. The steady solution will be helpful to quantify the convergence with respect to the height of the domain.

Let us recall that the traction boundary condition (3.8) is used on the exit section of the computational domain. As the reference flow is not known the choice is to take the flow just computed in the previous cell. If we think of a computation inside a channel the flow rate at the exit section must be equal to the upstream flow rate. Now the flow rate of the numerical flow computed in the previous row of cells is not strictly equal to the flow rate upstream and thus the flow rate can diverge slowly to another value yielding a mass variation. To avoid this drawback it is required to control the flow rate downstream at each time step. In a channel it is very easy but in an open domain like ours there are two choices as the flow on the top frontier is free to enter or to leave the domain. Either the flow rate downstream is controlled equal to the flow rate of the entrance section and the top frontier (Q1), or the flow
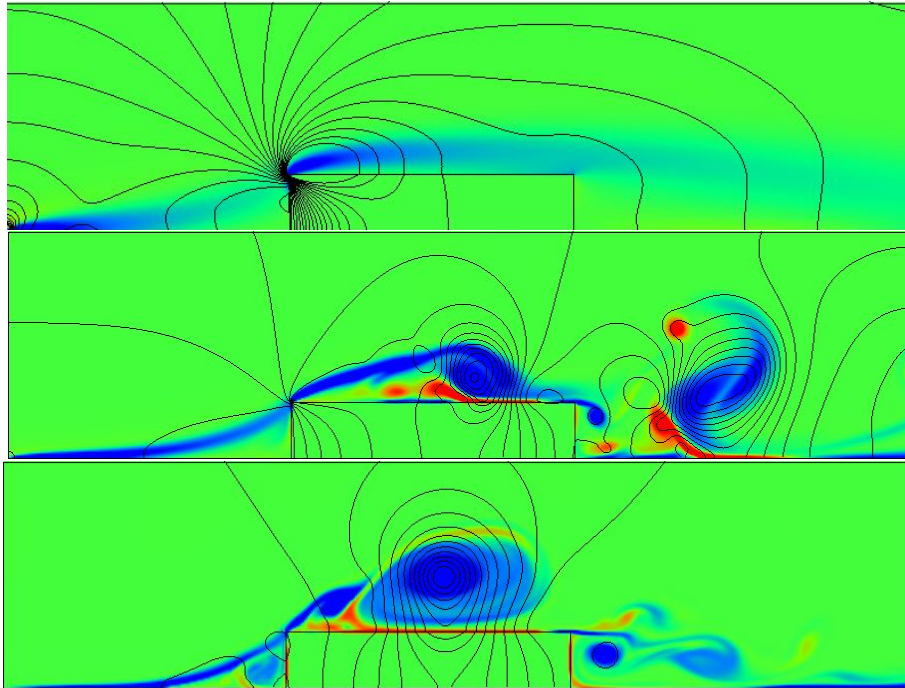
Figure 4. Vorticity field and pressure of the instantaneous flow by a long bar at $Re = 100$ (top) $Re = 1,000$ (middle) and $Re = 10,000$ (bottom) computed in the largest domain. Are plotted from blue to red the vorticity field in the interval (-5,5) and in black lines 25 pressure contours between -0.5 and 0.5 for $Re = 100$, between -2 and 2 for $Re = 1,000$ and between -6 and 6 for $Re = 10,000$.

rate on the top frontier and downstream is controlled equal to the upstream flow rate (Q2). That means that for Q1 we set:

$$Q_{in} = Q_{upstream} + Q_{top}, \;\; Q_{out} = Q_{downstream} \qquad (4.1)$$

and for Q2 we set:

$$Q_{in} = Q_{upstream}, \;\; Q_{out} = Q_{top} + Q_{downstream}. \qquad (4.2)$$

Then the flow rate control is achieved multiplying the velocity on the *out* part by the factor Q_{in}/Q_{out} to get the same flow rate than in the *in* part. The solutions of Figure 4 are computed with Neumann boundary condition and Q1 control. However at $Re = 100$ every boundary condition gives the same steady solution on the largest domain. For higher Reynolds numbers the stable solution is not steady anymore and thus the instantaneous solutions cannot be the same. However the mean flow is the same on the largest domain. In this section the computation of the mean flow is a very sensitive task and is performed generally using at least $50,000$ time iterations. Let us point out that, specially in two-dimensions, the flow is strongly linked to the size and strength of the vortices. Indeed, some events consisting of a large and strong vortex travelling through the second part of the domain can occur sometimes. This kind of event can last for thousands of time iterations and change the mean flow. This is particularly true for transitional flows at $Re = 1,000$ for instance as there are sometimes merging of several vortices. It is thus necessary to

compute several mean flows to avoid some events and to be careful analysing the results.

The aim of this work is to find out a boundary condition on Γ_S that allows the flow to leave or to enter the domain. So the first step is to check if the boundary conditions listed in the previous section satisfy this constraint. In Figure 5 are compared the Neumann, the traction, the Neumann with divergence-free, the extrapolation and the parabolized boundary conditions applied to the smallest domain ($h = 4$) to the reference flow obtain in the largest domain ($h = 128$). This comparison is performed with the flow rate all along the domain in the x-direction for two Reynolds numbers $Re = 100$ and $Re = 1,000$. Thus it is equal to 4 at the entrance section and should fluctuate further downstream. The results show that it is not the case for the Neumann with divergence-free boundary condition. The traction gives a small fluctuation of the flow rate whereas the other boundary conditions seem to better satisfy our demand although the results are not good. In particular the parabolized boundary condition does not converge on such a small domain and the extrapolation converges only at $Re = 100$.
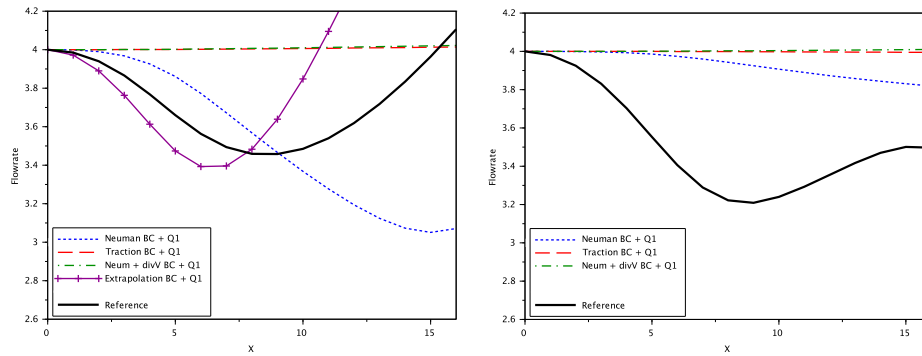

Figure 5. Comparison of the flow rate on the smallest domain for various boundary conditions at $Re = 100$ (left) and $Re = 1,000$ (right).
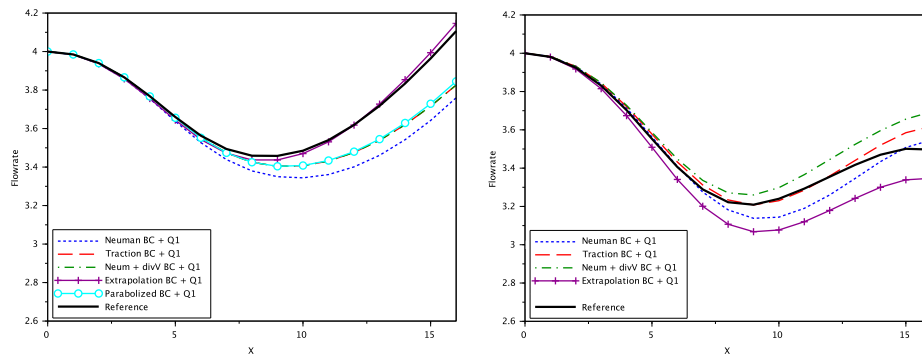

Figure 6. Comparison of the flow rate in the section $(0, 4)$ of solutions computed in the $h = 8$ domain for various boundary conditions at $Re = 100$ (left) and $Re = 1,000$ (right).

To further analyse the behaviour of the flow with respect to the boundary condi-

tions let us see in Figure 6 the flow rate always in the section $(0, 4)$ but for solutions computed in a larger but small domain with $h = 8$. At $Re = 100$ we see at first sight that the Neumann boundary condition gives the worst result, that the traction, the Neumann plus divergence-free and the parabolized boundary conditions give about the same result and that the extrapolation is almost superimposed to the reference solution. On the contrary at $Re = 1,000$ the Neumann boundary condition without or with divergence-free give quite poor results, the traction condition is closer to the reference, the parabolized condition is not stable enough to get a solution and the extrapolation is this time far to the solution. Let us point out that we use a linear extrapolation to guess the flow inside the ghost cell. At low Reynolds number there is a steady solution that evolves in the z-direction almost linearly in the vicinity of Γ_S, which is not the case for higher Reynolds numbers. The same findings are true on the domain with $h = 16$. So finally we decide to keep Neumann and traction boundary conditions and to discard the others.
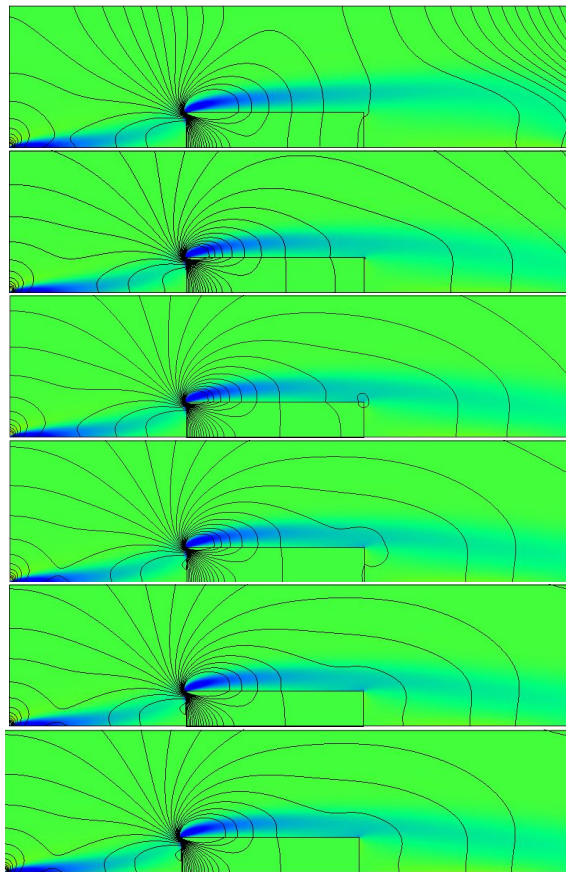

Figure 7. Comparison of the flow at $Re = 100$ for various height h of the domain. Are plotted from blue to red the vorticity field and in black lines the pressure contours. From top to bottom $h = 4$, $h = 8$, $h = 16$, $h = 32$, $h = 64$ and $h = 128$.

To quantify the convergence with respect to the height h of the domain, we plot in the domain $(0, 16) \times (0, 4)$ the steady solutions at $Re = 100$ computed for various h with Neumann boundary condition (see Figure 7). The solution in the smallest

domain is very far to the reference one as there is a kind of compression due to the small variation of the flow rate given by the boundary condition. The quality of the solution increases when h increases to give an almost converge solution at $h = 32$. Then the solutions for $h = 64$ and $h = 128$ are superimposed. This means that the convergence is really achieved for a blockage around $b = 1/50$ and thus a domain of height $h = 50H$, which is a lot! This is true for low Reynolds numbers as the diffusion effect is large, for higher Reynolds numbers it is smaller.

Now to see the influence of the height of the domain h to the quality of the numerical simulation, the flow rate is plotted always in the same section $(0, 4)$ along the x-direction whatever the value of h is. The results at $Re = 100$, $Re = 1,000$ and $Re = 10,000$ for the Neumann and traction boundary conditions are plotted in the Figures 8, 10 and 12 respectively. We see at a glance that the solution is always bad in the smallest domain. Then at $Re = 100$ the solution for both conditions goes monotonously closer to the solution as h increases. In addition, except for $h = 4$, the profiles at the middle of the bar are almost superimposed to the profile of the reference solution as shown in Figure 9.
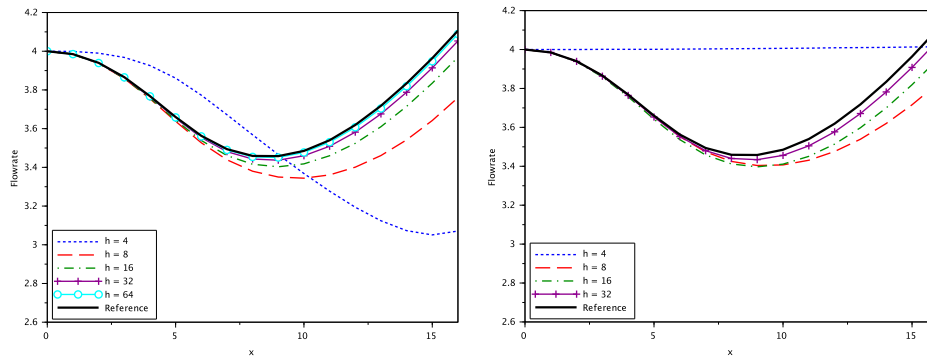

Figure 8. Comparison of the flow rate at $Re = 100$ in the section $(0 , 4)$ for various height h of the domain. The Neumann boundary condition (3.5) (left) or the traction boundary condition (3.8) (right) is used on the top frontier.

At $Re = 1,000$ the convergence is not monotonous any more when h increases. For instance the flow rate is worse for $h = 16$ than for $h = 8$ with Neumann boundary condition. In the same way the flow rate is very close to the reference flow rate for $h = 16$ with traction boundary condition whereas it is much less good for $h = 32$. The explanation is probably linked to the difficulty to get a good mean flow because of strong merging of vortices occurring sometimes. Surprisingly this is not observed at higher Reynolds number (see Figure 12). There are also larger discrepancies on the profile in the middle of the bar at $Re = 1,000$, specially just above the bar, than for $Re = 100$ or $Re = 10,000$ as shown in Figures 9, 11 and 13.

To summarise the discussion above in two-dimensions, two sets of boundary conditions are selected: the Neumann boundary condition (3.5) and the traction boundary condition (3.8). It is hard to say which one gives the best results but they do not give the same results even on a medium mesh. Indeed if we compare the results of Figure 10 for $h = 32$ at $Re = 1,000$ we see clearly that the flow rate for Neumann boundary condition is quite far to the reference for x between
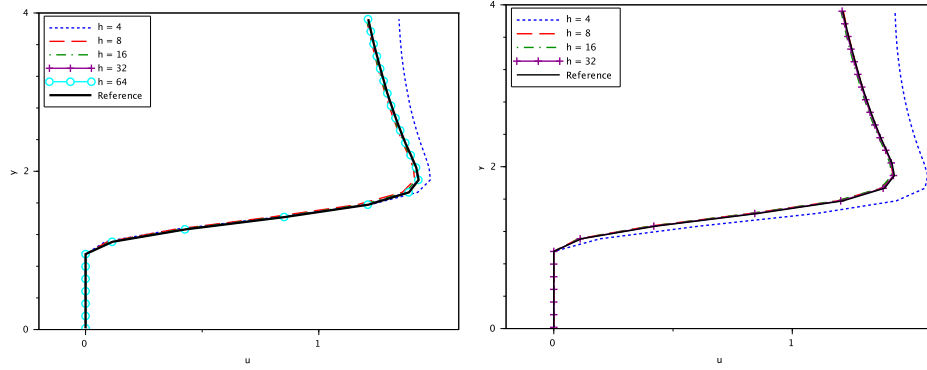
Figure 9. Comparison of the profile in the middle of the bar at $Re = 100$ for various height h of the domain. The Neumann boundary condition (3.5) (left) or the traction boundary condition (3.8) (right) is used on the top frontier.
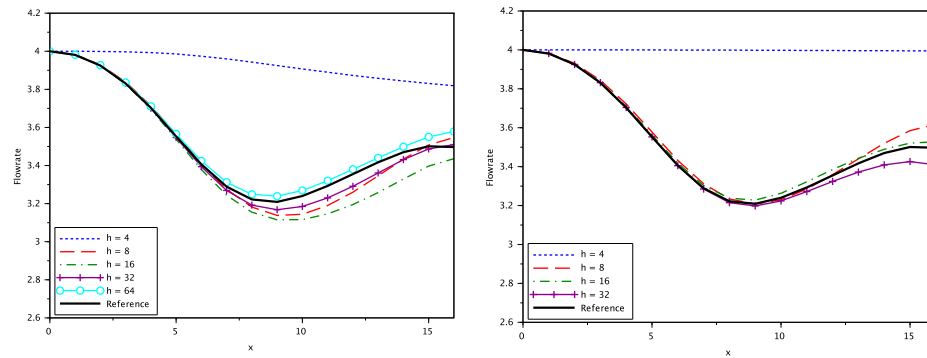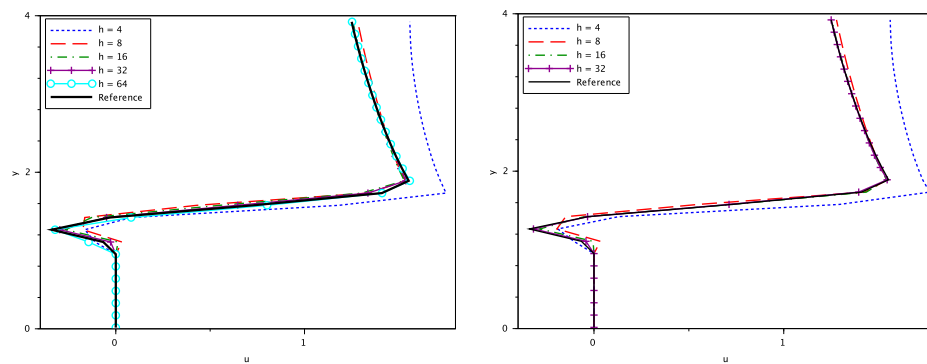

Figure 10. Comparison of the flow rate at $Re = 1,000$ in the section $(0,4)$ for various height h of the domain. The Neumann boundary condition (3.5) (left) or the traction boundary condition (3.8) (right) is used on the top frontier.

Figure 11. Comparison of the profile in the middle of the bar at $Re = 1,000$ for various height h of the domain. The Neumann boundary condition (3.5) (left) or the traction boundary condition (3.8) (right) is used on the top frontier.
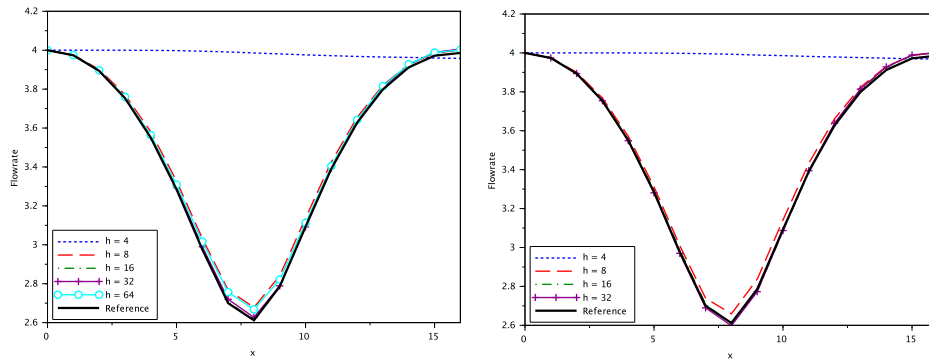
Figure 12. Comparison of the flow rate at $Re = 10,000$ in the section $(0, 4)$ for various height h of the domain. The Neumann boundary condition (3.5) (left) or the traction boundary condition (3.8) (right) is used on the top frontier.
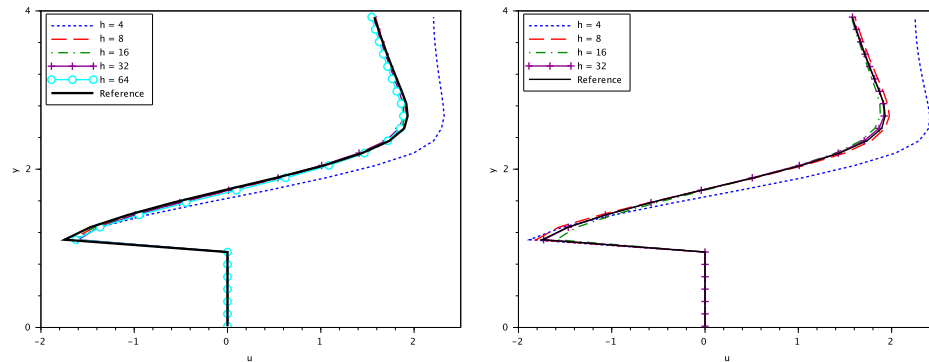

Figure 13. Comparison of the profile in the middle of the bar at $Re = 10,000$ for various height h of the domain. The Neumann boundary condition (3.5) (left) or the traction boundary condition (3.8) (right) is used on the top frontier.

8 and 13 and quite close at the exit section whereas the flow rate for traction boundary condition is very close to the reference until $x = 12$ and then diverges. These boundary conditions give converged results only when the blockage of the computational domain by the bar is around $b = 1/50$ at low Reynolds numbers. So it is required to put away the artificial frontier longitudinal to the flow while it is not necessary downstream with traction boundary condition that conveys properly the vortices downstream. At high Reynolds numbers good results are achieved with a higher blockage $b \simeq 1/15$.

There is another issue concerning the choice of the flow rate control. The results above are obtained with Q1 control but we propose to compare with Q2 control. At $Re = 100$ the results are almost superimposed except for $h = 4$ with Neumann boundary condition, thus it is not possible to determine which flow rate control is the best. At $Re = 1,000$ and $Re = 10,000$ there are significant discrepancies between the two controls as shown in Figures 14 and 15. At $Re = 1,000$ there are large differences with Neumann boundary condition whereas the difference occurs only in the vicinity of the exit section for traction boundary condition. On the contrary at

$Re = 10,000$ there are low differences with Neumann boundary conditions and quite large differences in the main part of the domain with traction boundary condition. It appears that with this last boundary condition the Q1 control is more efficient.
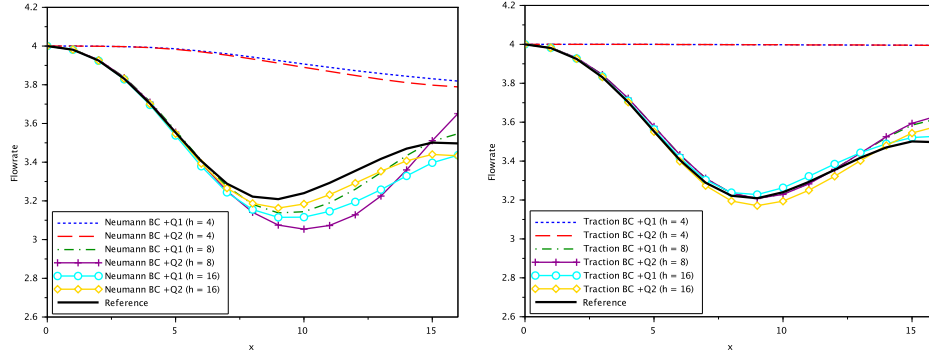

Figure 14. Comparison of the flow rate at $Re = 1,000$ in the section $(0,4)$ for various height h of the domain. The Neumann boundary condition (3.5) (left) or the traction boundary condition (3.8) (right) is used on the top frontier associated to Q1 or Q2 flow rate control.

Figure 15. Comparison of the flow rate at $Re = 10,000$ in the section $(0,4)$ for various height h of the domain. The Neumann boundary condition (3.5) (left) or the traction boundary condition (3.8) (right) is used on the top frontier associated to Q1 or Q2 flow rate control.
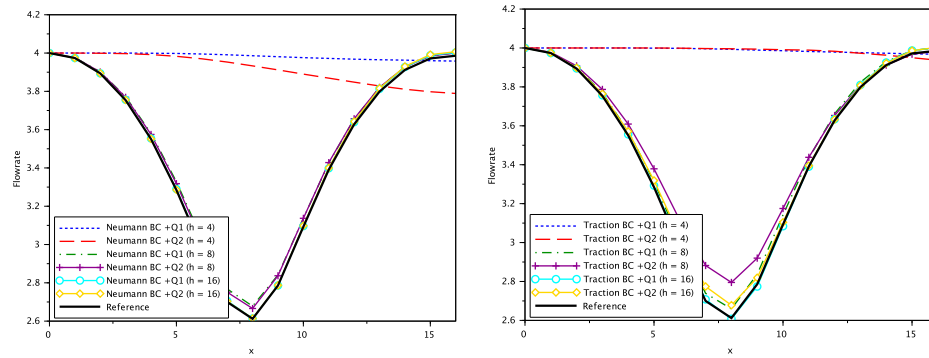
Another way to see the influence of the flow rate control is given in Table 1 that shows the mean drag coefficient of the bar when the boundary condition (3.5) or (3.8) is associated to Q1 or Q2 control. We see that in the smallest domain there is a significant difference between Neumann and traction boundary conditions results. For Neumann boundary condition there are quite large discrepancies according to the flow control but there are much less differences for traction boundary condition. In the domain with $h = 16$ the value are already quite close. So it is finally hard to say which control gives the best results. They seem to yield somehow equivalent results. Thus the quality of the solution is linked in priority to the distance of the top frontier Γ_S according to the Reynolds number Re. The higher the Re is, the closer Γ_S can be to the bar as the C_D value is already correct in the domain with $h = 8$ for $Re = 10,000$.

Table 1. Variation of the mean drag coefficient C_D of the long bar with respect to the size of the domain h and the Reynolds number Re for various boundary conditions in two-dimensions. For instance 4-N1 means $h = 4$ and Neumann boundary condition + flow rate control Q1. The values of the C_D in the largest domain with $h = 128$ for $Re = 100$, $Re = 1,000$ and $Re = 10,000$ are respectively 1.62, 0.86 and 0.14.

Re	4-N1	4-N2	4-T1	4-T2	8-N1	8-N2	8-T1	8-T2	16-N1	16-N2	16-T1	16-T2
100	1.52	1.63	2.06	2.06	1.50	1.50	1.55	1.55	1.57	1.57	1.56	1.56
1,000	1.96	1.58	2.24	2.25	1.21	1.22	1.10	1.10	1.02	0.97	0.91	0.98
10,000	0.90	1.58	0.55	0.56	0.13	0.13	0.13	0.16	0.13	0.14	0.13	0.17

5.   Numerical results in three-dimensions

Let us consider in this section the tree-dimensional flow around a long bar $(5 , 10) \times (h/2-1/2 , h/2+1/2) \times (0 , 1)$ of section 1 in the computational domain $\Omega = (0 , 16) \times (0 , h) \times (0 , h)$ where h takes the values $h = 4$, $h = 8$ and $h = 16$. These three values correspond to a blockage of the computational domain by the bar $b = 1/16$, $b = 1/64$ and $b = 1/256$. The study concerns three different Reynolds numbers $Re = 100$, $Re = 1,000$ and $Re = 10,000$ corresponding as in two-dimensions to three different regimes as shown in Figure 16. The drag coefficient of the long bar C_D corresponding to these three regimes is given in Table 2 and the flow rate in the section $(6, 10) \times (0, 4)$ with $h = 16$ in Figure 17. As in two-dimensions the variation is stronger at low Reynolds number as the diffusion term is higher.

Table 2. Variation of the mean drag coefficient C_D of the long bar with respect to the Reynolds number Re in three-dimensions.

Reynolds number	100	1,000	10,000
C_D	1.41	1.02	0.96

Taking into account the results of the previous section we have tested in three-dimensions the more relevant boundary conditions. The results of this section concern only Neumann boundary condition (3.5) with control of the flow rate downstream with respect to the other sides of the domain ($Q1$) or with control of the flow rate on the four open frontiers with respect to the flow upstream ($Q2$), and also the traction boundary condition (3.8) with the same two flow rate controls. In both cases we have to determine in addition to the two-dimensional unknowns, the unknown v in the y direction with the same formulas. For the traction boundary condition, this component v is computed in the z direction in the same way than u and is computed in the y direction using the divergence-free condition.

As in two-dimensions there are large discrepancies of the results with respect to the size of the domain or the blockage b. Here $h = 4$ is the smallest size and corresponds to an upstream flow rate $q = 16$ and a blockage $b = 1/16$, $h = 8$ corresponds to a blockage $b = 1/64$ and $h = 16$ corresponds to a blockage $b = 1/512$ that is large enough to be considered as the reference flow. Figure 18 shows clearly for two values of the Reynolds number that the solution is almost converged with $h = 8$ as the blockage is already low contrarily to two-dimensions. The same conclusion is reported for the vertical profile through the centre of the bar (see Figure 19). In addition this figure shows also that the flow at infinity is recovered much easily at high Reynolds number as there is less dissipation. Both the flow rate and the profile are computed on the mean solution computed when the regime is well established on $20,000$ time iterations. In three-dimensions the computation of
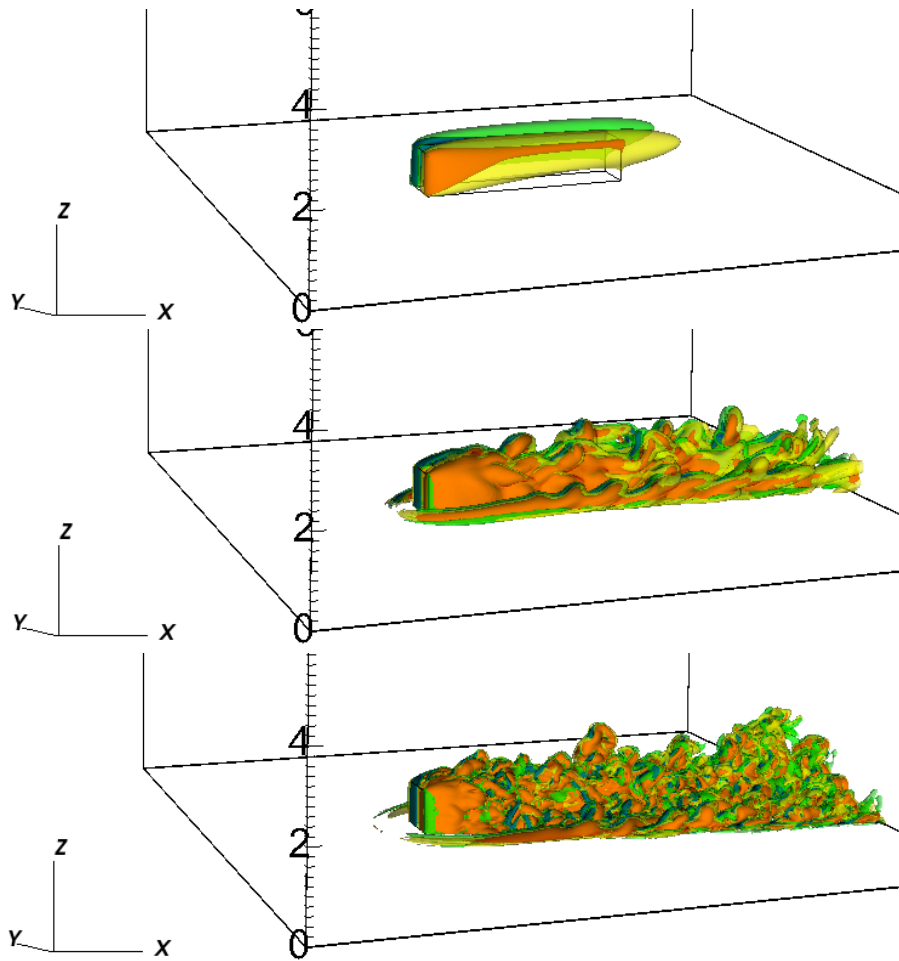
Figure 16. Vorticity field of the instantaneous flow by a long bar at Re=100 (top) Re=1,000 (middle) and Re=10,000 (bottom) computed in the largest domain in three-dimensions. From blue to red are represented four vorticity contours with values -2, $-2/3$, $2/3$ and 2.

the mean flow is less sensitive to the vortical structures as there is always a mixture of many vortical structures coming from various directions. Thus the mean flow is easier to get.

Let us now compare the boundary conditions. Hopefully the results are the same on the largest domain whatever the boundary condition is as shown on the profile in Figure 20. In fact, for high Reynolds number like $Re = 10,000$, as the flow at infinity is recovered closer to the bar it is possible to use the computational domain with $h = 8$. It corroborates the fact found in two-dimensions that the quality of the solution depends on the blockage and the Reynolds number. The Figure 21 shows clearly that both flow rate controls give the same result as the curve are superimposed. At low Reynolds number Neumann boundary condition gives results closer to the reference, for higher one it is about the same.

Another way to quantify the results is to compare the mean drag coefficient of the long bar with respect to the size of the domain h and the Reynolds number Re
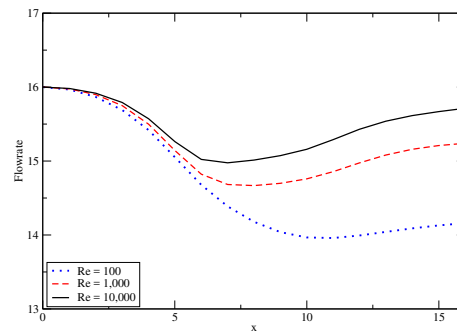
Figure 17. Comparison of the flow rate in the section $(6, 10) \times (0, 4)$ with $h = 16$ for various Reynolds number Re in three-dimensions.
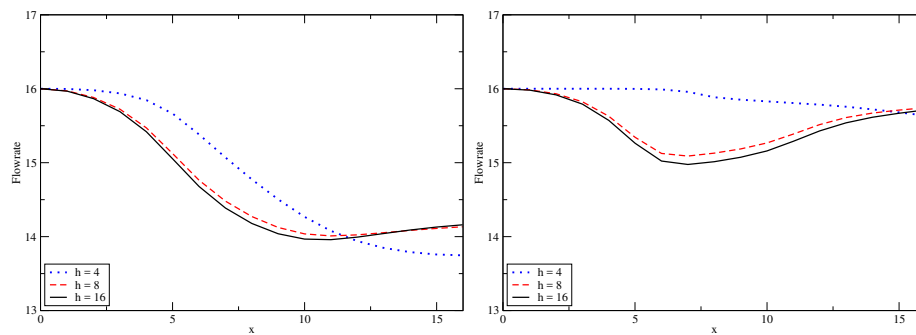

Figure 18. Comparison of the flow rate in the same section for various size of the computational domain. Flow in three-dimensions at $Re = 100$ (left) and flow at $Re = 10,000$ (right).
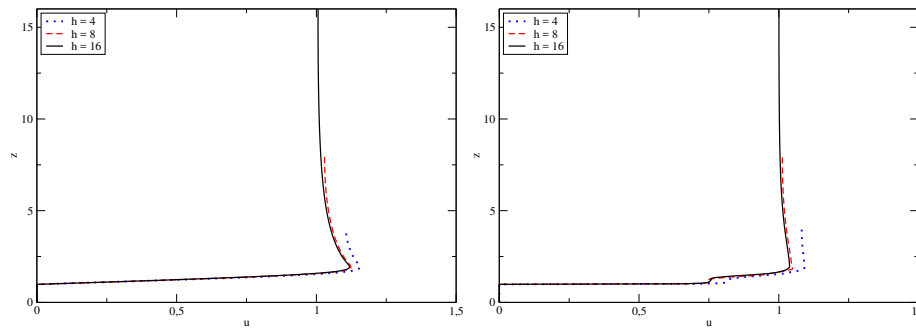

Figure 19. Comparison of the vertical profile through the centre of the bar for various size of the computational domain. Flow in three-dimensions at $Re = 100$ (left) and flow at $Re = 10,000$ (right).

(see Table 3). Let us first point out that the traction boundary condition does not converge in the smallest domain at $Re = 10,000$. In addition the results for the other values of the Reynolds number are better with Neumann boundary condition than with traction one. But the whole results are very close in the larger domains.
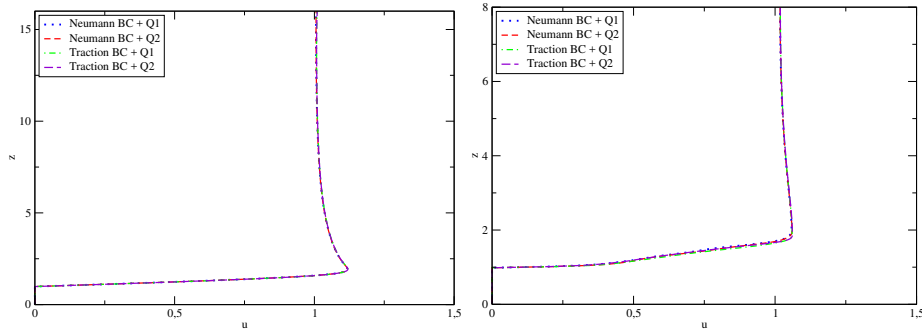
Figure 20. Comparison of the vertical profile through the centre of the bar for various boundary conditions. Flow in three-dimensions at $Re = 100$ in the largest domain with $h = 16$ (left) and flow at $Re = 1,000$ in the intermediate domain with $h = 8$ (right).
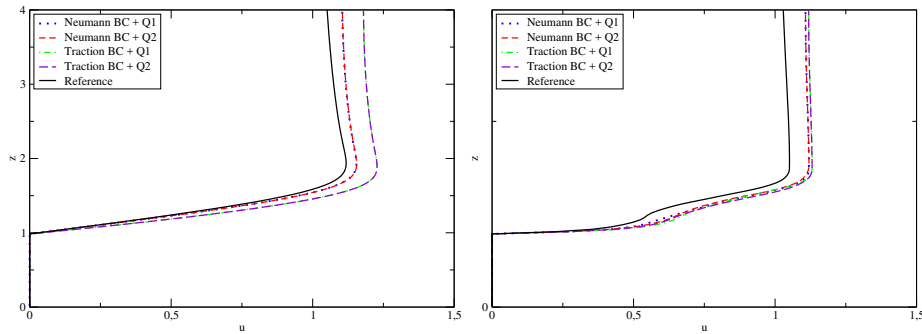

Figure 21. Comparison of the vertical profile through the centre of the bar for various boundary conditions. Flow in three-dimensions at $Re = 100$ (left) and flow at $Re = 1,000$ (right) in the smallest domain with $h = 4$.

Table 3. Variation of the mean drag coefficient C_D of the long bar with respect to the size of the domain h and the Reynolds number Re for various boundary conditions in three-dimensions. For instance 16-T2 means $h = 16$ and traction boundary condition + flow rate control Q2.

Re	4-N1	4-N2	4-T1	4-T2	8-N1	8-N2	8-T1	8-T2	16-N1	16-N2	16-T1	16-T2
100	1.43	1.44	1.87	1.87	1.42	1.42	1.48	1.48	1.41	1.41	1.42	1.42
1,000	1.15	1.16	1.20	1.20	1.04	1.04	1.04	1.04	1.02	1.04	1.02	1.02
10,000	1.01	1.01	-	-	0.96	0.96	0.96	0.98	0.96	0.95	0.95	0.96

6. Conclusions

In this work far field boundary conditions are tested to simulate the flow around one long bar set down on a wall in two- and three-dimensions. This work focus on the longitudinal artificial frontiers where the flow is almost tangent to the boundary. The study both in two- and three-dimensions shows that there are several boundary conditions that allow the flow to leave or enter the domain contrarily to Navier-slip boundary condition. Among these boundary conditions Neumann and traction boundary conditions give the more stable and reliable results. However at low Reynolds numbers the extrapolation can be a good choice.

The quality of the solution is linked to the blockage b of the computational domain by the obstacle in the direction transverse to the flow. It appears that a

ratio of about $b = 1/50$ is required to get fully converged results at $Re = 100$, which gives a strong constraint in two-dimensions. But this ratio increases with the Reynolds number and reaches $b \simeq 1/15$ at $Re = 10,000$. For larger values of b there is still a kind of compression of the flow that increases the drag coefficient of the body.

Acknowledgements

References

[1] P. Angot, C. H. Bruneau and P. Fabrie, *A penalization method to take into account obstacles in incompressible viscous flows*, Numer. Math., 1999, 81.

[2] C. H. Bruneau and P. Fabrie, *Effective downstream boundary conditions for incompressible Navier-Stokes equations*, International Journal for Numerical Methods in Fluids, 1994, 19(8).

[3] C. H. Bruneau and P. Fabrie, *New efficient boundary conditions for incompressible Navier-Stokes equations : a well-posedness result*, ESAIM: Mathematical Modelling and Numerical Analysis - Modélisation Mathématique et Analyse Numérique, 1996, 30(7), 23–28.

[4] C. H. Bruneau and K. Khadra, *Highly parallel computing of a multigrid solver for 3D Navier-Stokes equations*, J. Comp. Sc., 2016, 17(1).

[5] C. H. Bruneau and M. Saad, *The 2d lid-driven cavity problem revisited*, Computers & Fluids, 2006, 35(3), 326–348.

[6] C. Conca, F. Murat and O. Pironneau, *The Stokes and Navier-Stokes equations with boundary conditions involving the pressure*, Japanese journal of mathematics. New series, 1994, 20(2).

[7] B. Engquist and A. Majda, *Absorbing boundary conditions for the numerical simulation of waves*, Mathematics of Computation, 1977, 31(139).

[8] J. Filo and A. Zaušková, *2D Navier-Stokes equations in a time dependent domain with Neumann type boundary conditions*, Journal of Mathematical Fluid Mechanics, 2010, 12(1).

[9] G. Fournier, F. Golanski and A. Pollard, *A novel outflow boundary condition for incompressible laminar wall-bounded flows*, Journal of Computational Physics, 2008, 227(15), 7077–7082.

[10] L. Halpern and M. Schatzman, *Artificial boundary conditions for incompressible viscous flows*, SIAM Journal on Mathematical Analysis, 1989, 20(2), 308–353.

[11] L. T. Hoang, *Incompressible fluids in thin domains with Navier friction boundary conditions (i)*, Journal of Mathematical Fluid Mechanics, 2010, 12(3).

[12] M. Israeli and S. Orszag, *Approximation of radiation boundary conditions*, Journal of Computational Physics, 1981, 41(1), 115–135.

[13] G. Jin and M. Braza, *A nonreflecting outlet boundary condition for incompressible unsteady Navier-Stokes calculations*, Journal of Computational Physics, 1993, 107(2).

[14] H. O. Kreiss, *Initial boundary value problems for hyperbolic systems*, Communications on Pure and Applied Mathematics, 1970, 23(3), 277–298.

[15] Y. Li, J. Choi, Y. Choic and J. Kim, *A simple and efficient outflow boundary condition for the incompressible Navier-Stokes equations*, Engineering Applications of Computational Fluid Mechanics, 2017, 11(1).

[16] N. Masmoudi and F. Rousset, *Uniform regularity for the Navier-Stokes equation with Navier boundary condition*, Archive for Rational Mechanics and Analysis, 2012, 203(2).

[17] R. L. Sani and P. M. Gresho, *Résumé and remarks on the open boundary condition minisymposium*, International Journal for Numerical Methods in Fluids, 1994, 18(10).

[18] G. Zhou and N. Saito, *The Navier-Stokes equations under a unilateral boundary condition of Signorini's type*, Journal of Mathematical Fluid Mechanics, 2016, 18(3).